PERGAMON

Applied Geochemistry 15 (2000) 667–686

Applied Geochemistry

Regional fluid characterisation and modelling of water–rock equilibria in the Boom clay Formation and in the Rupelian aquifer at Mol, Belgium

C Beaucaire[a,*], H. Pitsch[a], P. Toulhoat[a], S. Motellier[a], D. Louvat[b]

[a]*Commissariat a l'Energie Atomique, DCC/DESD/SESD,Laboratoire d'étude de l'interaction roche–eau, CEA-Saclay, 91191 Gif sur Yvette, France*

[b]*Commissariat a l'Energie Atomique, DCC/DESD/SESD, Laboratoire de géosciences, expérimentation et modélisation, CEA-Cadarache, BP No. 1, 13108 Saint Paul Lez Durance, France*

Received 5 March 1999; accepted 16 June 1999
Editorial handling by W.M. Edmunds

Abstract

Interstitial water from the Boom clay Formation around the HADES (high activity disposal experimental site, an underground research facility belonging to the Nuclear research centre, SCK·CEN, at Mol-Dessel, Belgium.) underground research facility at Mol, Belgium, and waters sampled at different locations in the Rupelian aquifer, underlying the clay formation, have been studied. The Boom clay is a Tertiary mudrock containing about 55 % clay and the Rupelian aquifer is located in a silty layer. Special care was taken to adapt or improve measurement, sampling, conservation and analysis methods to get a reliable regional and local database, for the purpose of testing a general model describing the regulation and acquisition of the composition of these fluids. The isotopic and chemical composition of the waters allows them to be assigned to a common origin, namely mixing between a marine endmember and the clay interstitial water, followed by reequilibration with the host rock through dissolution–precipitation reactions involving identified secondary minerals. Oxidation–reduction state and trace element behavior are also discussed and the limits of the model are outlined.

1. Introduction

Within the research programmes concerning the performance assessment of underground radioactive waste disposal, the Boom clay Formation in Belgium has been investigated for more than 15 a, in order to evaluate its capacity to host such a repository and play a significant role as a geological barrier against the migration of radionuclides towards the ecosphere. One of the key issues of this characterisation effort is the prediction of the behavior of potentially dangerous elements, which could be solubilized in the groundwater. Their movement will depend both on the regional hydrology and on the chemical interaction with dissolved species and minerals of the host rock. The objective of the work presented here is to understand the mechanisms of the acquisition and regulation of the groundwater composition in this massif, in order to set a comprehensive basis for such predictions and

* Corresponding author. Tel.: +33-1-6908-3233; fax: +33-1-6908-3242.
E-mail address: catherine.beaucaire@cea.fr (C. Beaucaire).

0883-2927/00/$ - see front matter
PII: S0883-2927(99)00067-0

at the same time to contribute to a general modelling of the chemical composition of groundwaters in clays.

Interstitial water from the Boom clay Formation sampled from the HADES underground research facility at Mol-Dessel, Belgium, and waters from the Rupelian aquifer, underlying the clay formation, have been studied. In the whole paper 'interstitial water' will refer exclusively to the water extracted from the clay. Sampling and analytical methods have been developed and adapted to take into account the specific constraints of a clay massif with a relatively high water content (20%), poorly buffered in terms of acidity and oxido-reduction potential; one major objective was to limit the perturbations induced by the methods used, in order to improve the accuracy of the determinations. The acquisition of numerous data from the 7 successive campaigns and the continuous sampling in the underground laboratory have provided a regional and local database. Part of the results presented here were communicated at WRI-8 in Vladivostok, Russia (see Beaucaire et al., 1995; Pitsch et al., 1995a,b).

These data were used to extend and verify a model describing the regulation and acquisition of the chemical composition of the different waters. The hypothesis was made that sedimentary fluids like the ones investigated here could reach their prevailing chemical composition in the same way as granitic waters (Grimaud et al., 1990): progressive dissolution of the host rock by the recharge water and successive precipitation of secondary minerals. The coexistence of several dissolution–precipitation equilibria fixes the concentration of a series of 'controlled elements', other ones remaining 'free', that is with a concentration depending only on the dilution of the corresponding recharge water.

The assumption that fluids from the Boom clay massif and from the underlying Rupelian aquifer can be considered as a group of similar waters relies on previous work concerning the regional lithostratigraphy and hydrology, synthesized in a recent work (Wouters and Vandenberghe, 1994). Boom clay was deposited from the sea, which occupied a large part of the north of Europe, 30 to 36 Ma ago. The formation belongs to the same Rupel group as the underlying silty layers of the Ruisbroek sands and the Bilzen Formation (Berg sands) which host a single aquifer, referred to as the 'Rupelian aquifer' in the rest of this paper. The Boom clay crops out along a NW–SE line passing near Mechelen and becomes confined towards the northeast of the Belgian Campine and The Netherlands with a pending of approximately 0.25%. The explored area, the Campine province, extends some 120 km (E–W) and 60 km (N–S) around the Mol-Dessel nuclear research centre, which hosts the HADES underground facility. A schematic SW–NE cross section is presented in Fig. 1.

The Boom clay contains mainly clay minerals dominated by illite (about 60%), quartz (some 20%) and feldspars (5 to 10%). Other important secondary minerals are carbonates and pyrite, which indicates that reducing conditions are prevailing (Wouters and Vandenberghe, 1994; Griffault et al., 1996). The relative proportions of the phases vary according to the fine stratification of the clay, which is related to the turbulence regime during sedimentation (Vandenberghe and Van Echelpoel, 1987); the most silty fractions also contain glauconite. Qualitatively, a similar mineralogy is observed in the Ruisbroek and Berg sands regarding the main phases: quartz is the most abundant, clay,

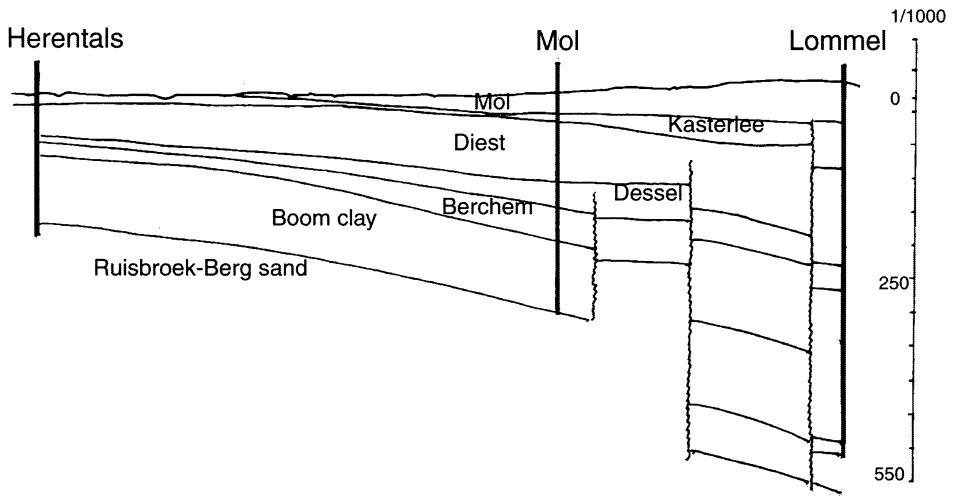

Fig. 1. Schematic cross section from SW (left) to NE (right) through the investigated formation. The broad vertical lines represent drill-holes. Depth in meters.

carbonates and glauconite the most important secondary minerals.

2. Sampling and analytical techniques

Some of the interstitial water samples were collected from 2 piezometers (denoted No. 1 and 2) equipped with filters at different depths in the massif: 3, 7, 8, 10, 14 and 15 m starting from the HADES gallery which is located at 223 m below ground level. Setting up of the piezometers and sampling was performed by SCK·CEN staff (Griffault et al., 1996). Other samples were extracted by squeezing the clay at the British Geological Survey (BGS, Keyworth, Great Britain). Samples from leaching experiments carried out at the Bureau de Recherches Géologiques et Minières (BRGM) were also examined. To provide consistency, all the analyses were carried out in the same laboratory (CEA·LIRE), except those of the squeezed water, which were analysed at the BGS. A reference sample was analysed in both laboratories: the results showed good agreement (4% average deviation). All groundwaters of the aquifers were collected by CEA·LIRE from the drill-holes belonging to SCK·CEN.

2.1. Sampling techniques

2.1.1. Interstitial water

These samples were collected under vacuum in stainless steel cells kept at 4°C and directly connected to the drains from the piezometer filters at different depths. This arrangement ensured that the sampling conditions were anaerobic. Pressure gauges connected to the cells made it possible to control the filling of the cells by observing the pressure increase up to that of the massif at the considered depth. The flow rates of the 14–15 m and 7–8 m filters were 1 and 0.5 ml/h, respectively. The fluids were further handled in the laboratory without exposure to O_2. 80 ml were collected in each cell, 50 ml of which were reserved for dissolved sulphide analyses, the residue being divided in two fractions, one filtered (0.45 μm) and acidified (pH 2–3) for cation analysis, the other filtered but nonacidified for anion analysis and measurement of the alkalinity. The interstitial water samples assigned to trace element analysis were collected from a specific piezometer equipped with a system of nylon dialysis membranes. This was found to give a 3-fold decrease of the Fe concentration with respect to that from the water sampled using stainless steel cells.

2.1.2. Groundwater from the aquifers

Samples of this water were collected with a device that brings a water column from the desired depth to the surface by applying a N_2 pressure, after a series of cleaning cycles. The pH, Eh and temperature measurements were made at the site. The samples were conditioned as described above (filtration, acidification) and kept at 4°C until they were analysed.

2.2. Filtration techniques

The degree to which the samples are representative of the groundwater and the quality of the measurements depends to a large extent on the sampling techniques and the precautions taken in sample treatment, particularly in the filtration stage. A convenient filtration threshold must be maintained, redox conditions have to be controlled and the samples must be preserved from contamination or mineral precipitation. Both interstitial and aquifer water samples were subjected to a series of sequential filtrations as follows:

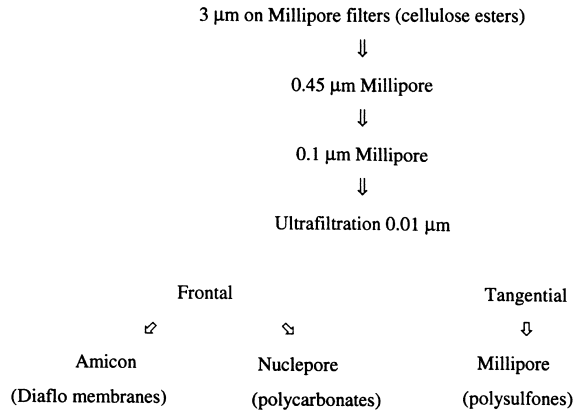

Sequential filtration relies on a succession of decreasing porosity filtrations of the same sample; an aliquot of the filtrate is taken from each step for analysis. This technique was preferred to parallel filtration since it minimises clogging, which is the main process that increases the retention of particles below the filtration threshold. Due to the constraints of working in the field, the sample concentration filtration mode was used (decreasing sample volume during the operation) although it is known that this operating mode can result in a modification of the solution equilibria (Buffle et al., 1992), in contrast to the diafiltration mode (conservation of a constant volume above the membrane). To minimize secondary effects, only an aliquot of the sample was filtered.

Nuclepore filters were selected because of their high pore size homogeneity. The filtration units were washed in a clean room in a 2N HNO_3 bath, then rinsed 3 times with ultrapure water. The filters were then stored in a refrigerator in Petri boxes sealed with Parafilm® until opening at the site. Similarly, the sto-

rage polycarbonate flasks were conditioned under Ar in sealed plastic bags.

The last step in the sequential procedure was an ultrafiltration with a porosity of 0.01 μm. Frontal ultrafiltration was performed with Amicon supports rinsed once with 0.1N HCl followed by MilliQ grade ultrapure water. Only 80% of the total sample was filtered to minimise the concentration effect. Tangential ultrafiltration was carried out using a Minitan system (Millipore).

At each filtration step, the first few milliliters were discarded.

To limit any oxidation, which can affect elements like Fe, all the samples were kept under an Ar atmosphere during the filtrations. Each receiver was filled with Ar before sample addition and the numerous decantings were also carried out under an inert atmosphere. However, in spite of all these precautions, ferric hydroxide formation could be observed during the filtration of the most acid samples.

2.3. Analytical methods

2.3.1. Chemical analysis

Alkalinity, HS, RS, S_2O_3, SO_3: Potentiometry (in a N_2 atmosphere)
Tacussel TT-processor II
Ingold combined pH electrode
AgS electrode + Tacussel Ag/AgCl reference; buffers for pH = 7 and pH = 11

Co, Ni, Zn: Cathode stripping voltammetry
Tacussel POL 150 polarograph + MDE 150 stand
Dimethylglyoxime + ammonium buffer

H_4SiO_4: UV-VIS Spectrometry
Perkin–Elmer Lambda 5 absorption spectrometer
Ammonium molybdate, ascorbic acid, oxalic acid, tin (IV), acetic buffer

UO_2: Fluorescence spectrometry
Scintrex UA 3 Analyser
Dilor time-resolved laser fluorescence spectrometer + Sopra laser ($\lambda = 337$ nm)
Fluorescence reagent: FLURAN (Scintrex)

Al, Fe, Mn, Pd: Graphite furnace atomic absorption spectrometry
Perkin–Elmer 2380 + HGA 400 programmer
Zeeman effect Unicam 939 QZ

Li, Na, NH_4, K, Mg, Ca; F, Cl, Br, NO_3, PO_4, SO_4: Ion-exchange chromatography
Dionex 4500i with conductimetric detection + CSRS-I (cations) and ASRS-I (anions) electrochemical suppression modules
Columns: Dionex CS12 (cations) or AS4A (anions)
Eluents: methanesulfonic acid (cations) and carbonate + bicarbonate (anions)

2.3.2. Isotopic measurements

2.3.2.1. Stable isotopes. The heavy isotope concentrations are defined in differences per mil (δ‰) with respect to a standard, which, for ^{18}O and ^{2}H, is standard mean ocean water (SMOW), for ^{13}C, a cretaceous marine calcite (Pee Dee Belemnoïde Formation, PDB), and for ^{34}S, sulphur from a meteorite (Canyon Diablo troilite, CD). The ratio of the heavy isotope to the common isotope of the element was obtained by gas mass spectrometry. The uncertainty in the measurements is ±0.1‰ for $\delta^{18}O$, ±1.0‰ for $\delta^{2}H$ and ± 0.3‰ for $\delta^{13}C$ and $\delta^{34}S$.

2.3.2.2. Tritium. The ^{3}H concentration in natural water was measured, after electrolytical enrichment, by liquid scintillation counting, or with a gas proportional counter when the sample was too small to be enriched. Error bars are given for each sample. These concentrations are given in ^{3}H units (TU): 1 TU corresponds to 1 ^{3}H atom per 10^{18} atoms of H or an activity of 0.11 $Bq.l^{-1}$.

2.4. pH measurements

WTW pH-millivoltmeter with a Pt temperature detector
Ingold combined electrode

Similar results were obtained either measuring the pH in a ground neck tube (stationary sample) or in an autothermostated flow cell (125 ml, in-cell flow rate 0.5 l/min) directly connected to the water sampler outlet. However, it must be stated that in both cases the sampled water was certainly perturbed after being subjected to pressurised N_2 for at least 10 min during sampling with the collecting device. Thus, partial degassing of dissolved CO_2 cannot be excluded and the measured pH values are likely to be overestimates of the real pH (see below, Section 3). More accurate values of the pH could be obtained only by in situ measurements.

2.5. Redox potential measurements

2.5.1. Electrode potential and equilibrium potential

An inert electrode, i.e. that exchanges only electrons, takes a stable equilibrium potential when immersed in a solution which contains at least one oxidizing and one reducing species in sufficiently high concentrations (5 μM for an electrode with a surface area of a few mm^2) which belongs to the same redox couple. Two species of different couples may also impose a stable mixed potential to the electrode, if the reducing species is oxidized at a lower potential than the reduction potential of the oxidizing species. In both cases the current-potential curve at this electrode has a well defined intersection with the potential axis which corresponds to the potential measured at zero current with a millivoltmeter and the same indicator electrode.

In all other cases, the current-potential curve shows a broad zero-current plateau, which can extend up to the limits of the electroactivity field of the water-electrode system in the absence of electroactive species. The potential measured in the classical way is then unstable, since very small perturbations (concentration fluctuations, electrode surface modifications...) make the potential 'jump' from one value to another within this plateau: the solution is not buffered from the oxidation–reduction point of view.

In addition to the time-stability criterion, the coincidence of the values measured with different inert electrodes allows one to confirm the existence of an equilibrium potential, unique and independent of the nature of the measuring electrode.

2.5.2. Flow cell measurements

2.5.2.1. Equipment

Tacussel Ionoprocessor + UCE switching unit + printer + Servotrace registrator
Tacussel DEL 1 Teflon electrochemical detection cell for HPLC (volume of 50 *μl*)
Indicating disk electrodes: Pt ($\phi = 2$ mm), vitreous C (VC, $\phi = 2{,}5$ mm), Au ($\phi = 3$ mm)
Ag/AgCl reference electrode

The cell was enclosed in a Faraday cage connected to the metallic piezometer by a grounding braid. It was connected to the piezometer at the 15 m level by a 4 m long, 0.1 mm diameter Teflon tube in order to reduce the outlet pressure of the fluid. The metal electrodes were cleaned with emery paper, then washed successively with HNO_3, acetone and ethanol before insertion in the cell.

2.5.2.2. Experiment. The potential measurements in the interstitial water lead to values much higher than those expected for this type of fluid: this suggests an oxidizing perturbation, possibly in the Teflon tubing which is slightly permeable to O_2. The affected species could be sulfides or Fe (II). However, the residence time is short — 2 min — with respect to the known reaction half-lives (Liyuan Liang et al., 1993), even if it must be noted that in the present case the contact surface/solution volume ratio is doubtless larger than that in the cited work.

On the other hand, there is no signal stabilisation nor convergence of the 3 measured potentials, even after more than 300 h, which raises serious doubts as to the existence of an equilibrium potential in the water that circulated in the cell. Signal drift and especially the 'jumps' characteristic of an unstable mixed potential situation were observed, confirming the erratic results of batch measurements. These observations have been confirmed by plots of current-potential curves with rotating electrodes of the same type as the indicator electrodes, for interstitial water samples kept under N_2. All the curves exhibit a plateau of several hundred millivolts where the recorded current is very low, showing that no electroactive species are concentrated enough to impose a stable zero-current potential.

3. pH of the interstitial water

3.1. In situ measurements with an optical sensor

3.1.1. Experimental device

This system has been described elsewhere (Boisde and Perez, 1988; Motellier et al., (in press)). A

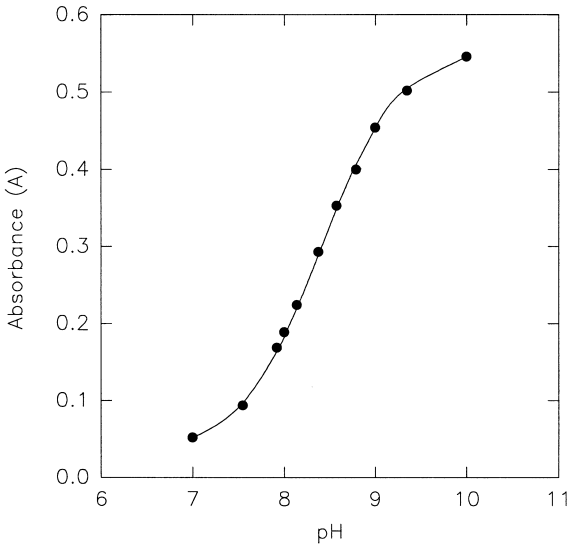

Fig. 2. Calibration of the optode.

coloured pH indicator was adsorbed on a hemispherical bead of resin tightened at the end of a 20 m-long optical fibre (optode). A portable spectrophotometer (Optolec H), equipped with electroluminescent diodes of wavelengths adapted to the indicator, was connected to the optode to monitor the absorbance versus pH. The main characteristics of the device are:

Dimensions: L = 20 m; ϕ_{max} = 4.0 mm
Indicator support: 1/2 bead of XAD4 resin, ϕ = 1.2 to 1.4 mm
Indicator: phenolsulfonephthalein (phenol red)
pH range: 6–10 (linear between 7.5 et 9.0)
Response time: 20 min.

After washing the optode with ethanol and rinsing it with deionised water, it was inserted in specially designed tubing to the last chamber (14 m) of piezometer No. 2. The system, up to the filter chamber, was sealed by a Swagelok® connector with a Teflon® fitting. Correlation of the absorbance signal with the pH of the water in the piezometer chamber was obtained by calibration with a series of 11 buffers (Fig. 2).

3.1.2. In situ measurements

The in situ measurement lasted some 200 h with a frequency of one acquisition per hour. During this period, the piezometer was opened and thus depressurised once, which made it possible to renew the water near the indicator, at the end of the fibre. An electrical fault stopped the acquisition after 200 h; the pressure had then reached its nominal value of 17.6 bar. The optode was, however, not withdrawn until after 13 days in the piezometer.

The variation of the pH and pressure with time are shown in Fig. 3, for the duration of the in situ monitoring. The initial pH was 8.6 which corresponds to a partially degassed solution but less than that of samples taken at atmospheric pressure, for which the measured pH is around 8.6–8.8. The pressure drop accompanying the piezometer purge is marked by an absorbance increase signifying an excursion to a more alkaline medium, due to partial degassing. Stabilisation of the signal took some 130 h, which is due to the very low hydraulic conductivity of the medium: 10^{-12} m s^{-1}. The average absorbance value beyond this stabilisation period led to a definite pH value of 8.21 (standard deviation = 0.05%).

3.2. Measurement with a flow cell

3.2.1. Experimental equipment

Tacussel ISIS 20000 pH-millivoltmeter
Kipp and Zonen registrator
Flow cell with a combined glass electrode, connected to the piezometer by 4 m long, 0.1 mm diameter Teflon tubing to reduce the fluid pressure; in-cell flow rate: 0.8–0.9 ml/h.
Bioblock NBS type buffers were used to control the pH:

pH = 6.86 at 25°C: 0.025 M KH_2PO_4 and 0.025

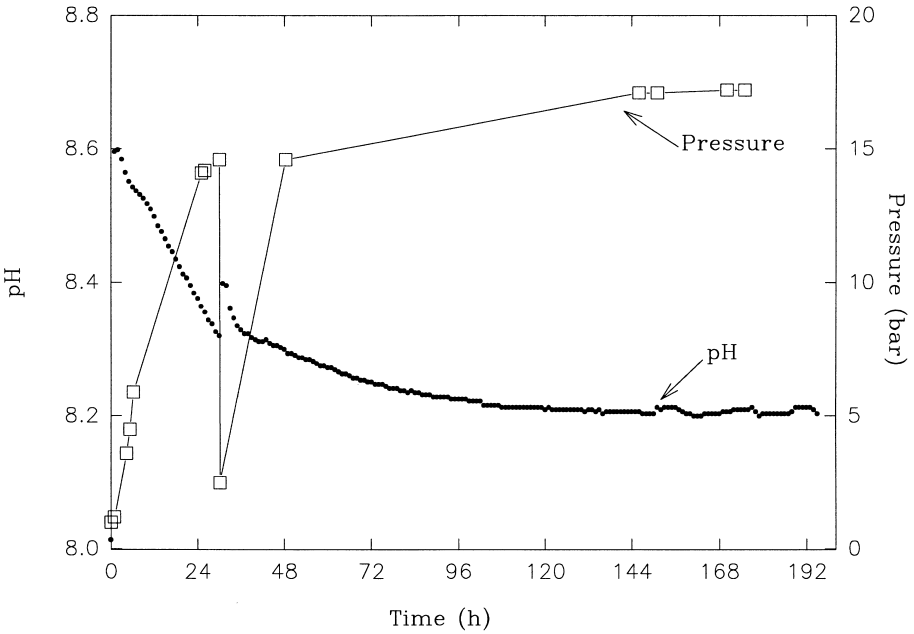

Fig. 3. Variation of the optode signal and the pressure with time.

M Na_2HPO_4 ($\mu = 0.1$ M)
pH = 9.18 at 25°C: 0.01 M $Na_2B_4O_7,10H_2O$ ($\mu = 0.02$ M)

3.2.2. pH measurement

The pH was continuously monitored for 14 days. A two point calibration was carried out before the measurement by introducing the buffer solutions using a piston pump with a 20 ml/h flow rate. At the end of the experiment, the pH of the two buffer solutions were measured again, showing a remarkable stability of the measurement chain (differences of respectively −0.01 and +0.02 pH units, after 339 hours).

The variation of the measured pH with time is shown in Fig. 4. It increases quickly up to 8.41, then slowly decreases after 50 h, that is after 45 ml of fluid has passed through the cell. This volume corresponds to 90% of the volume of the piezometer tubing. Due to the very low hydraulic conductivity of the medium, stabilisation of the signal takes about 185 h, until the piezometer and the tubing have been purged twice. The average of the values beyond this limit is: $pH = 8.191 \pm 0.003$ (95% confidence interval).

3.3. Accuracy and precision of pH measurements

The overall time-dependences of the signals obtained with the flow cell and the optode are similar. Clearly, the initial rise corresponds to a delay in the reequilibration of the water contained in the piezometer (slow redissolution of the CO_2 which was released by the decompression after opening). Regarding the final result, and assuming the worst, the flow cell value could be too high (due to possible partial degassing resulting from the pressure drop), the one measured by the optode is accurate or slightly too low if the remanence of the pressure effect on the bead is not complete: in consequence, 8.20 can reasonably be admitted as accurate.

As far as precision is concerned, the experimental confidence interval is markedly lower than the uncertainty on the pH due to its 'operational' definition (Robinson, 1980; Covington et al., 1985) which is, for such dilute solutions, of ±0.05 units. Thus it can be certified for the interstitial fluid:

$pH = 8.20 \pm 0.05$.

The calculated value for the interstitial water pH agrees with this result. If the same calculation is made fixing the CO_2 partial pressure at 3×10^{-4} atm, pH = 9.26 is obtained, that is a variation of more than a unit by assuming equilibration with the atmosphere. In fact, the values obtained from batch measurements are intermediate between these two limits: they correspond to partially degassed water. Besides this bias, these values are also scattered because the solutions are not in equilibrium with the atmosphere and because the time at normal pressure before pH measurement could vary to a large extent. The amplitude of the variations is related to the fact that the pH of the interstitial water, withdrawn from the massif, is not buffered. The fluid is roughly equivalent to a solution of $NaHCO_3$ and is thus very sensitive to any base or acid contamination or to the release of the dissolved carbonic acid, as is shown in Fig. 5.

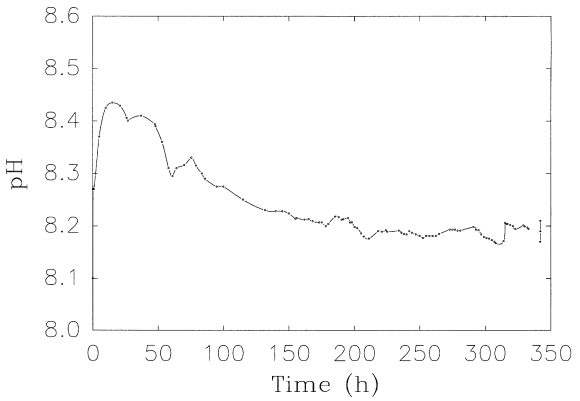

Fig. 4. Variation with time of the pH measured with the flow cell. The bar represents ±0.02 units around 8.19.

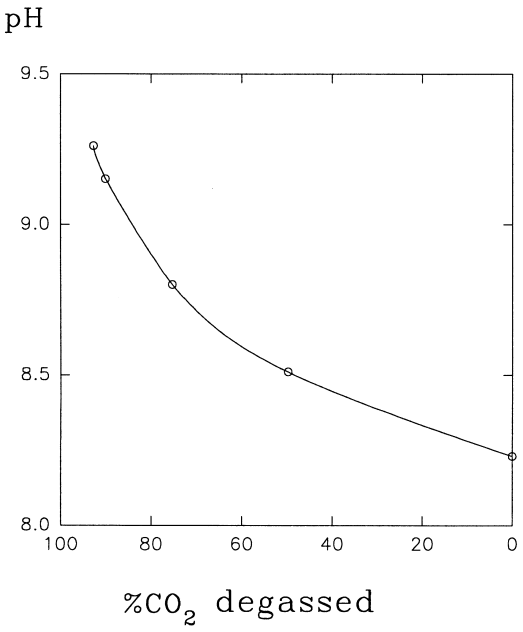

Fig. 5. Variation of the pH of the interstitial clay water by degassing of the dissolved carbon dioxide.

Table 1
Chemical composition of the clay interstitial water and the aquifer waters. Only the variations above 5% over the period 1991–1993 are indicated. Reference for piezometer No. 1 is the sampling distance from the gallery wall; n.d.: non determined

	Ref.	Depth (m)	pH		Anions				Cations								
				Alkalinity (mmol/l)	SO_4 (mmol/l)	Cl (mmol/l)	Br (mmol/l)	SiO_2 (mmol/l)	Na (mmol/l)	K (mmol/l)	Ca (mmol/l)	Mg (mmol/l)	Li (mmol/l)	Al (μmol/l)	Fe (μmol/l)	Mn (μmol/l)
Drill holes (Rupelian aquifer)																	
Mol	15B	270	8.8–8.6	17.9–15.8	0.013–0.12	0.77	0.04	0.15	17.2	0.25–0.19	0.16–0.51	0.04–0.09	7.2–5.5	0.25	1.6–3.4	3.8–4.9
Wuustwezel	19E	225	6.9–7.6	3.2–2.9	1.48–2.08	1.05–4.24	0.06–0.012	0.16	1.25–16.8	0.30–0.40	2.20–1.15	0.66–0.59	2.9–14	< 0.02	1.8	7.9
Kontich	18B	61	8.7–7.9	6.7–6.6	0.05–1.5	1.41–2.34	< 0.0006	0.20	5.0–5.7	0.65–0.61	0.81–0.68	0.68–0.64	4.3–2.9	n.d.	0.2–0.5	2.5–5.3
Herentals	1C	195	8.6–8.4	12–11.3	0.17	5.75	0.009	0.16	16.9–17.8	0.29–0.39	0.17–0.27	0.17	9.5–14.5	0.078	1.5	4.5–1.5
Poppel	42D	486	7.9–8.7	6.6–6.0	0.3–0.1	21.1–9.9	0.03	0.21	25.5–15.1	0.33	0.73–0.47	0.45	8.7– < 1	< 0.02	2.2	3.1
Oelegem	41C	131	7.6–8.1	14.2	0.12–0.41	23.8	0.037	0.17	37.4	0.82–0.65	0.15–0.48	0.16–0.44	28.8	n.d.	0.5	2–1.6
Lommel	12 F	480	9.5	12.5	< 0.0002	38	0.06	0.03	54.6	0.50	0.12	0.27	15.9	0.05	0.07	0.098
Meer	20D	358	7.7–7.8	13.2	4.09	92.7–96.7	0.12–0.19	0.21	102–110	1.37–0.90	0.60–0.80	1.30–1.80	43–72	< 0.02	0.1–0.5	1.3
Interstitial water (Boom clay)																
Piezometer 1	7–15	223	8.2	12.2	0.04	0.50	0.007	0.15	12.3	0.21	0.048	0.070	4.3	n.d.	2.9	2.75

4. Evolution of the groundwaters and modelling of water–rock equilibria

4.1. Main features of the water chemical composition

Analytical results are presented in Table 1. The interstitial water sampled from the Boom clay is equivalent to a $NaHCO_3$ solution with alkaline pH (8.2). It has a low SO_4 and a high Br content. Since the piezometers were installed, the chemical composition of this water has been remarkably constant. In the Rupelian aquifer, the water changes from $NaHCO_3$ water (Mol 15B, Cl: 0.77 mM, pH: 8.6), with nearly the same composition as that of the interstitial water, to NaCl water, with the highest concentration found in the Meer borehole (Cl: 96 mM, pH: 7.8). The pH decreases with increasing Cl concentration; in contrast, dissolved SO_4 increases from 0.01 up to 4 mM in the water with the highest Cl concentrations.

The general evolution of these fluids can be represented from correlations of major cations with the Cl or Na concentration (Fig. 6). Up to anion concentrations of 20 mM, HCO_3 is the predominant anion; they are progressively overtaken by Cl ions and the Na is thus balanced by the Cl with an excess [Na]/[Cl] ratio close to 1. The variations in the other cations are correlated with the Na with ratios that are different from those observed in seawater. The mixing trend with a marine endmember is also indicated in Fig. 6. For the less concentrated solutions, some scatter is seen corresponding to a fresh recharge influence (Wuustwezel, Kontich), labelled by seaspray contamination. Thus it is clear that the marine contribution cannot be excluded, in particular for elements such as Ca and Mg. However, beyond 20 mM Na, the observed correlations cannot be explained by a simple mixing with sea water.

The sea water contribution in the Rupelian aquifer is also evidenced in the variation of the concentrations of conservative ions such as halides. The representative content of the atmospheric recharge (surface water, 19E) and most of the Rupelian samples, 20D, 12F, 41C, 42D and 1C fall on the seawater dilution line (Fig. 7). The points representing Boom clay water and water from the Mol borehole are off this line ('Clay fluids' and '15B' respectively).

The representative points of samples recovered from leaching of clay with demineralised water or from squeezing are also shown in Fig. 7. Although the measured Cl^- concentrations are comparable to those obtained for the piezometer water (Clay fluids) the results cannot be interpreted for the Br^- concentrations. It must be concluded that these techniques for extracting water from clay induce chemical fractionation and that this fractionation seems to increase with the ionic radius of the species considered.

In the Rupelian groundwater, the $[Br^-]/[Cl^-]$ ratio clearly shows the marine contribution to the water salinity while in the interstitial water this ratio would appear to be representative of the clay–water interaction. Figure 8 confirms that ion concentrations observed in the Mol 15 B borehole result from a mixing between a 'clay water' component and a surface water recharge, whose ion concentrations reflect a marine environment (probably seaspray). As for Kontich 18B, the Cl^- enrichment with respect to Br^- could be due to leaching of evaporite formations by the groundwater in the southern border of the Rupelian aquifer system or by contamination from another aquifer.

The correlation of the concentrations of Br^-, normalised to that of Cl^-, which is conservative, and of SO_4, which is sensitive to biochemical phenomena, is shown in Fig. 9. It provides evidence of the large variations in SO_4 content of samples with a marine contribution. These variations give an evolutionary path between sea water and sample 12F which can be attributed to an increasing bacterial reduction of dissolved SO_4. A second reduction line can also be drawn between the water recharged locally, that of borehole

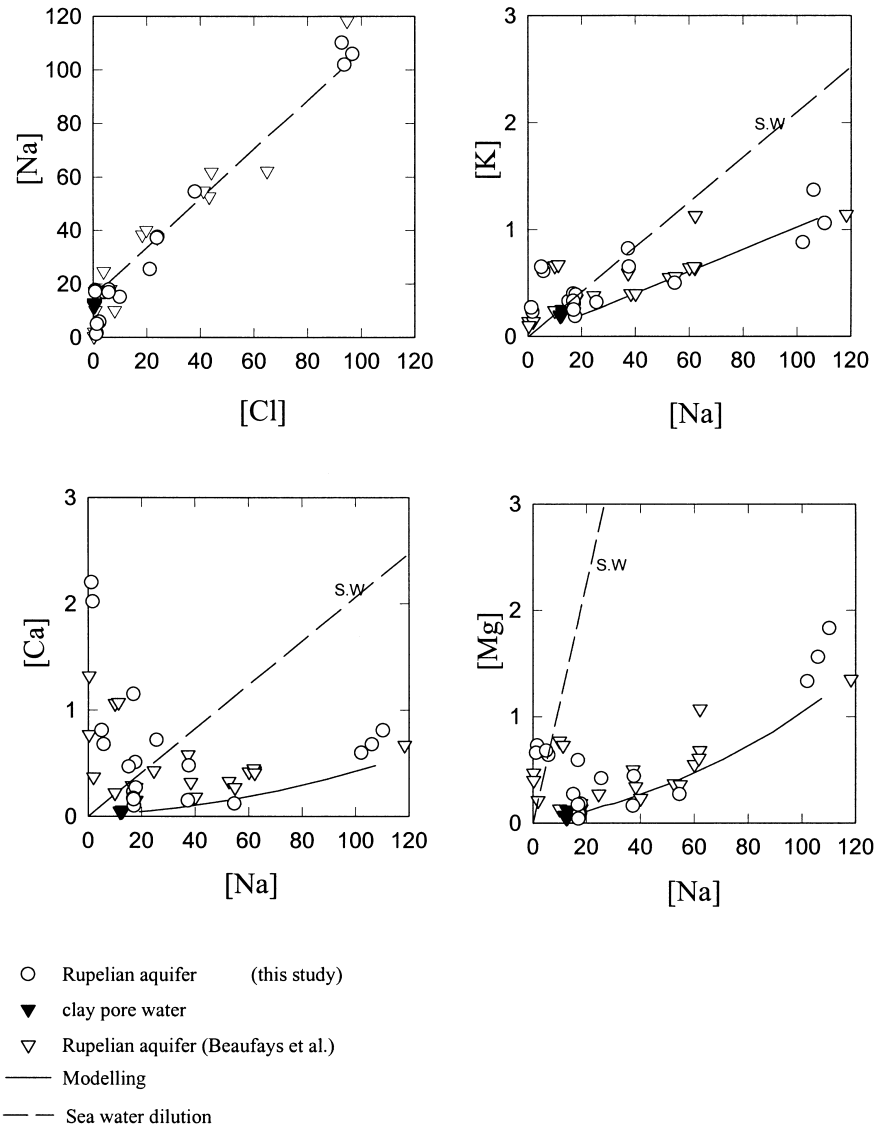

Fig. 6. Na-chloride, K, Ca and Mg-Na correlations in interstitial clay and aquifer waters. Concentrations in mM. The dotted straight lines (SW) represent the dilution of seawater. The solid lines indicate the modelling of the fluids at equilibrium with the assemblage: kaolinite, chalcedony, albite, microcline, calcite, dolomite (see Section 4.3).

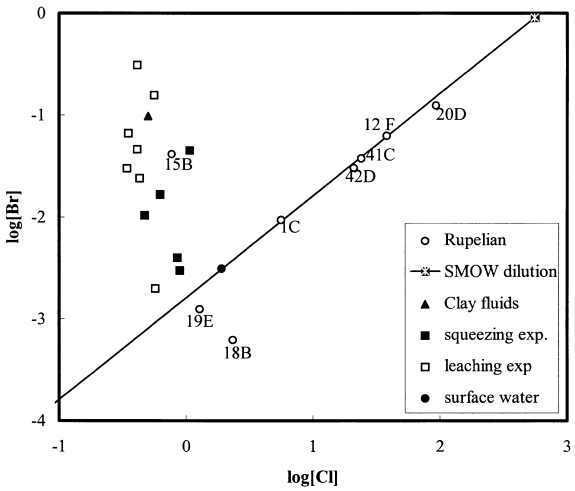

Fig. 7. Cl-Br correlations in interstitial water from piezometers in the Boom clay (clay fluids) from clay squeezing (squeezing exp.) or from clay leaching (leaching exp.) and the Rupelian aquifer samples. Concentrations in mM.

19E and the interstitial water. The dissolved SO_4 isotopic contents confirm these differences in SO_4 origins and the subsequent reduction phenomena.

The mineralisation of the Rupelian groundwater results from the superimposition of mineralisation largely originating from a mixing with a marine component and mineralisation due to water–rock interactions, which modifies the water cationic content.

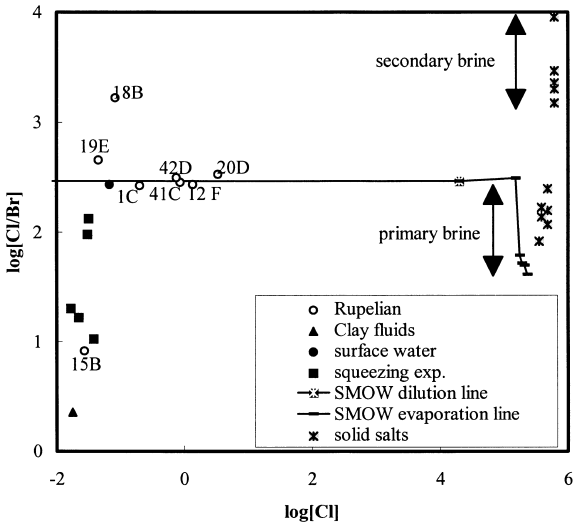

Fig. 8. Cl-Cl/Br correlations in interstitial water from piezometers in the Boom clay (clay fluids) or from clay squeezing (squeezing exp.) and the Rupelian aquifer samples. SMOW and brine data fromFontes and Matray, 1993. Concentrations in ppm.

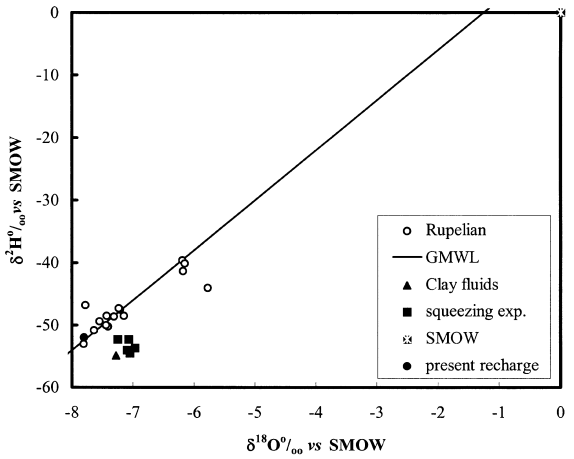

Fig. 10. $^{2}H-^{18}O$ correlation in interstitial and aquifer water.

4.2. Fluid origins and dynamics

The complete isotopic data are given in Table 2. The ^{18}O and ^{2}H contents representative of the Rupelian aquifer recharge are shown in Fig. 10. Except for the Meer 20D and Poppel 42D samples, all data are in a range of values close to those presently measured for atmospheric precipitations at the Groningen station (IAEA, 1992). It can thus be concluded that the recharge conditions are either those of present day or climatically little different from these. The content of stable isotopes in the groundwater samples between 1992 and 1994 reported in Table 2 remains stable over this time range. The ^{18}O content of the samples is even

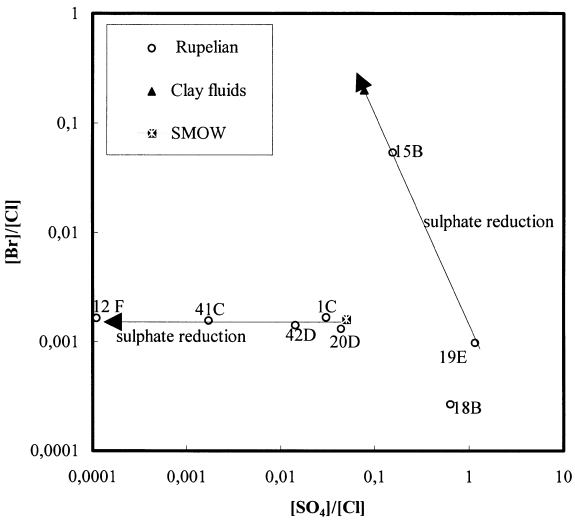

Fig. 9. Correlation of the bromide and sulfate concentrations, normalised to chloride, in the interstitial and aquifer water. Concentrations in mM.

Table 2
Isotopic data for interstitial clay water and aquifer water. δ represents the deuterium excess and is interpreted with respect to the global meteoric water line (GMWL) for which $\delta = 10$

Ref.	Date	Ref. Loc.	^{18}O water (‰ vs SMOW)	^{2}H water (‰ vs SMOW)	δ	^{3}H (TU)	^{13}C citd (‰ vs PDB)	^{18}O sulf (‰ vs SMOW)	^{34}S sulf (‰ vs CD)
1C	06-92	Herentals	−7.64	−50.8	10.3	0.6 ± 0.3			
1C	06-93	Herentals	−7.41	−50.2	9.1		−10.0		
15B	06-92	Mol	−7.81	−53.0	9.5	1.1 ± 0.7			
15B	06-93	Mol	−7.78	−46.8	15.4	0.6 ± 0.4	−11.1		
20D	06-92	Meer	−6.15	−40.1	9.1	0.6 ± 0.3		20.53	68.4
20D	06-93	Meer	−6.19	−39.6	9.9	1.0 ± 0.4	−12.4	21.83	69.4
19E	06-92	Wuustwezel	−7.55	−49.4	11.0	27.4 ± 0.9		6.33	−14.3
19E	06-93	Wuustwezel	−7.43	−48.5	10.9	20.2 ± 0.8	−10.0	6.99	−14.6
41C	06-92	Oelegem	−7.31	−48.6	9.9	0.0 ± 0.3			
41C	06-93	Oelegem	−7.44	−50.0	9.5	0.8 ± 0.4	−7.9		
18B	06-92	Kontich	−7.23	−47.3	10.5	0.6 ± 0.3		10.2	
18B	06-93	Kontich	−7.21	−47.5	10.2		−17.4	10.6	
12F	06-93	Lommel	−7.15	−48.5	8.7	3.5 ± 0.5	−3.1		
42D	06-93	Poppel	−6.18	−41.3	8.1	1.7 ± 0.5	−15.8		
42D	06-94	Poppel	−5.77	−44.0					
P1.8m	10-92	Interst. water	−7.28	−54.9	3.3				

comparable to the measurements of Beaufays et al. (1994a) made in 1985 and not reported in Fig. 10 because of the lack of corresponding ^{2}H data.

The 20D and 42D samples are different from the rest of the group in having higher heavy isotope contents with such a ^{2}H excess that the data plot under the Global Meteroric Water Line. This position is indicative of a process, which has modified the isotopic composition of the recharge water. In the present case Fig. 11, which combines the chemical and isotopic data, clearly shows that it is the mixing between the recharge water and a marine component already identified by the halides that modifies the water isotopic content of these two samples. This definitely proves

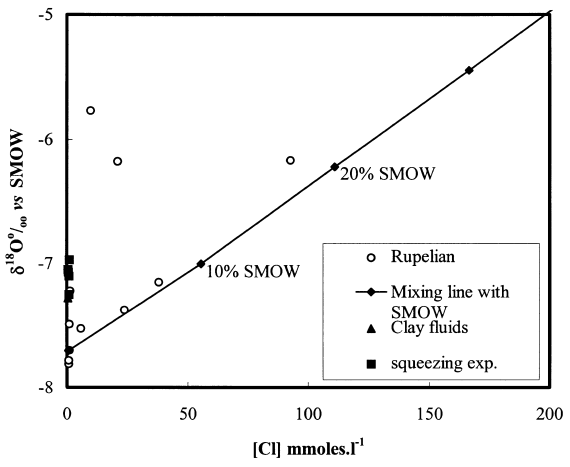

Fig. 11. ^{18}O-[Cl] correlation in interstitial and aquifer water.

that the mixing occurred between two water masses. In sample 20D, the proportion of sea water is around 15 to 20%. The samples 41C (Oelegem) and 12F (Lommel) also fall on this mixing line at lower sea water contributions. Therefore, part of the Rupelian aquifer Formation has been in contact with Holocene sea water.

From the beginning of the Rupelian groundwater chemical survey in 1985 (Beaufays et al., 1994a), it has been observed that the general evolution of this water remained the same with a saline front coming from the NE of the aquifer (Fig. 12). The water with the highest Cl content corresponds generally to the deepest levels of the aquifer (Meer 20D, Poppel 42D and Lommel 12F).

From a dynamics viewpoint, the absence of ^{3}H and the low radiocarbon activities of the total dissolved inorganic C (TDIC) show the magnitude of the transit time in the Rupelian. The zero ^{3}H contents give mean transit times above the recent period (the last 60 a) and the estimation of this time by Beaufays et al. from ^{14}C data goes up to the limit of the method, with mean transit times from 30 to 40 ka for the samples from the western part of the basin (1C, 15B, 20D and 41C).

However, local variations in the chemical composition of this water with time can be significant. This is seen in the eastern part of the basin, which is close to the Rupelian recharge areas. A constant evolution of the water from the Poppel 42D borehole is observed, with decreasing Cl concentrations (64.7 to 9.9 mM) and increasing heavy isotope contents. This increase can, therefore, no longer be related to the sea water

contribution. It could represent an evaporation effect affecting the recharge before its infiltration (transit through a lake or a river). The ^{3}H content, low but significant, the variation of the Cl (dilution) and the isotopes show a recent recharge in this part of the aquifer.

Similarly, Lommel 12F is now characterised by a very high silica deficit and would appear to be linked to a carbonate reservoir, which is confirmed by the increase of the TDIC ^{13}C content from −11 to −3‰ between 1985 and 1993. The ^{3}H concentrations in the water are now significant. In this case, the existence of appreciable fracture zones in the east of the reservoir, which were again active in the last seismic events (1993), could be the cause of a modification or an acceleration of the recharge.

Significant fluctuations in Cl in the Wuustwezel 19E borehole appear to be linked to a connection with surface aquifers. The ^{3}H concentration confirms the arrival in the boreholes of water from surface horizons labelled by ^{3}H resulting from surface thermonuclear tests. On the basis of the tritium records established for NW Europe (IAEA, 1992) and following the considered model (partial or total contribution of the modern recharge), the average transit time of this sample is estimated to be between 15 and 30 a. This modern recharge contribution could be seen in 1985 since the ^{14}C activity of the TDIC obtained in that borehole region was 85 pmc (percent modern C), which corresponds, after geochemical corrections, to a modern ^{14}C content. This contribution of recent water in the Rupelian appears to be a local phenomenon, probably linked to the integrity of the 19E borehole.

The isotope concentrations in the interstitial water samples collected either from piezometers or by squeezing fall under the GMWL (Fig. 10). This posi-

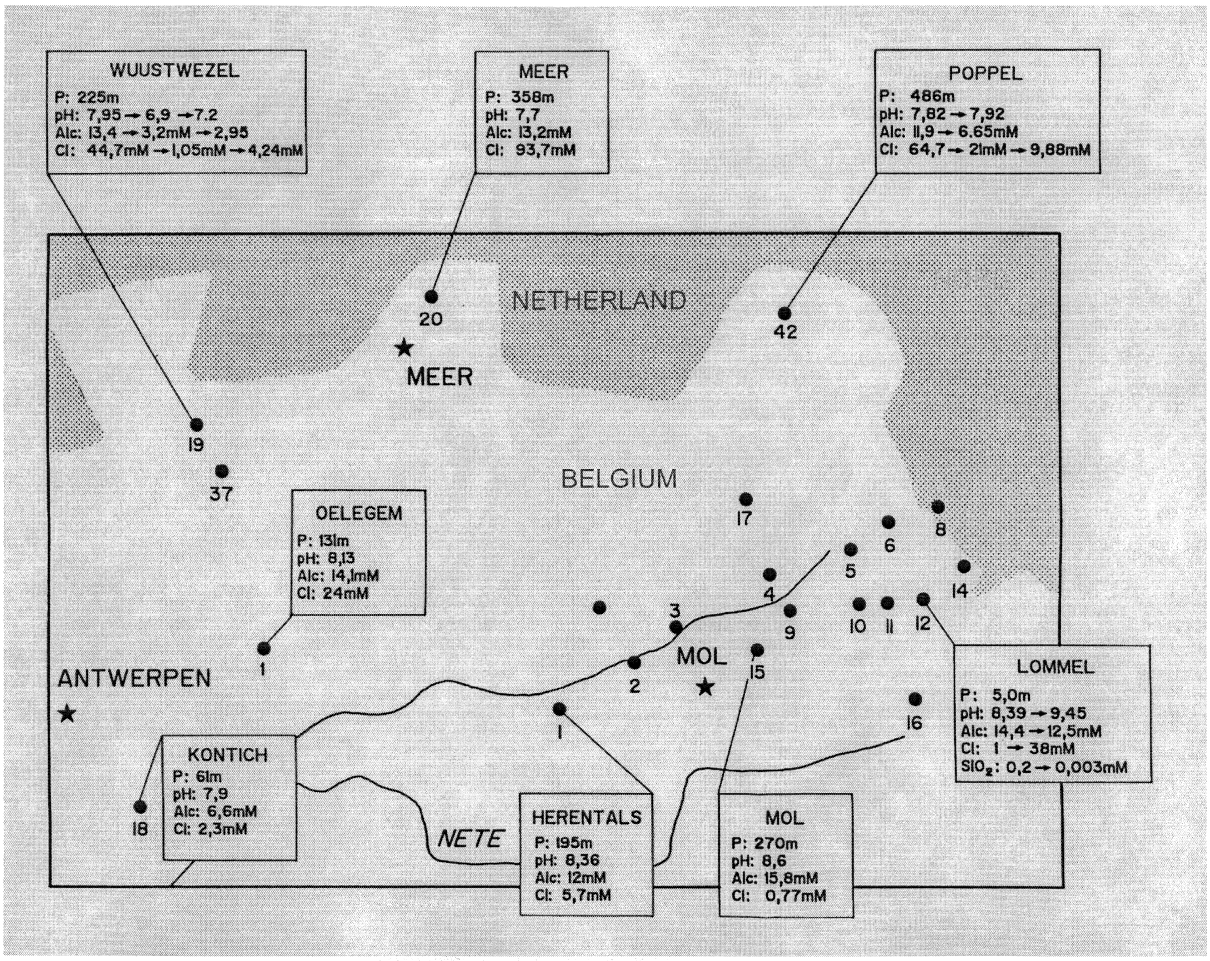

Fig. 12. Borehole emplacements in the Rupelian aquifer; the arrows indicate the variation of chemical compositions with time, including data from Beaufays et al. (1994a).

tioning is frequently observed for water extracted from clayey formations. The ^2H depletion has been noted to be an extraction artefact when the vacuum distillation technique is used to obtain water from clay (Araguas et al., 1995). Both methods used here to recover water from the Boom clay, gravity collection and squeezing extraction, could have fractionated the water stable isotope content.

4.3. A regional model for the major components

4.3.1. Principles of the chemical control

As previously mentioned, evidence has been provided for a two component mixture: one represented by the interstitial water and the Mol borehole water, the other by a marine component (i.e. 16% sea water) within the Meer borehole. However, a conservative mixing model does not account for the changes in Na, Ca, K and Mg suggesting that reequilibration of the fluids with their host-rock has occurred. Therefore, the aim is to establish the regulating mechanisms, taking into account the chemical evolution of both Rupelian aquifer fluids and clay pore waters, considering that these different waters have the same origin.

One of the major characteristics of these waters is the relatively high organic and inorganic C content: from 12 to 18 mM of HCO_3 and 0.3 mM to 10 mM of total organic C. The CO_2 values are between 10^{-3} atm (Mol, Herentals) and 10^{-2} atm (Meer, Oelegem), significantly above that corresponding to equilibrium with atmosphere. The majority of the fluids are close to saturation, or even supersaturated with the associated carbonate minerals: calcite, dolomite, siderite and rhodocrosite (Table 3). This relative supersaturation has not been completely explained; it could result from an overestimation of the pH data due to degassing during sampling (see above).

The examined waters are all saturated with chalcedony except for the one in the Lommel borehole which has a silica deficit and a very alkaline pH (>9) (Table 3). Due to the detection limit in the analysis for dissolved Al (4.10^{-8} M), its concentration could be determined only in the Mol 15B borehole. The value here appears to be consistent with the stability field generally defined for kaolinite (Michard, 1983). The other fluids can reasonably also be assumed to be at saturation with kaolinite.

On the other hand, excluding the boreholes recently disturbed such as Wuustwezel (surface contribution), and also the Lommel borehole (silica deficit), the fluids evolve from the interstitial water to a chlorinated one in keeping the (Na)/(H) and (K)/(H) ratios constant, suggesting a control by the solid phase on the solution chemistry (Fig. 13). All the existing data for the interstitial and Rupelian aquifer water are plotted, including those from Beaufays et al. (1994a). The scatter of the points is probably related to the recorded hydrodynamic fluctuations, the difficulty of determining the pH of fluids from considerable depths as well as to the

Table 3
Degree of saturation of the waters with respect to calcite, dolomite, chalcedony, siderite and rhodocrosite. Data from the June 1993 run. The saturation indexes are defined as follows: log (ionic product/solubility product)

	calcite	dol.	chalced.	sider.	rhod.
Mol 15B	1.11	1.44	0.11	0.06	1.03
Wuustwezel 19E	−0.76	−2.00	−0.021	0.005	−1.21
Kontich 18B	0.47	0.92	0.05	−1.03	0.21
Herentals 1C	0.54	1.05	−0.03	−0.29	0.89
Poppel 42D	0.24	−0.78	0.14	−0.57	−0.23
Oelegem 41C	−0.37	−0.65	−0.04	−1.08	−0.36
Lommel 12F	0.82	2.03	−0.82	−0.6	−0.27
Meer 20D	−0.007	0.31	0.19	−2.03	−0.8
Interstitial clay water	0.19	0.44	−0.09	−0.21	0.95

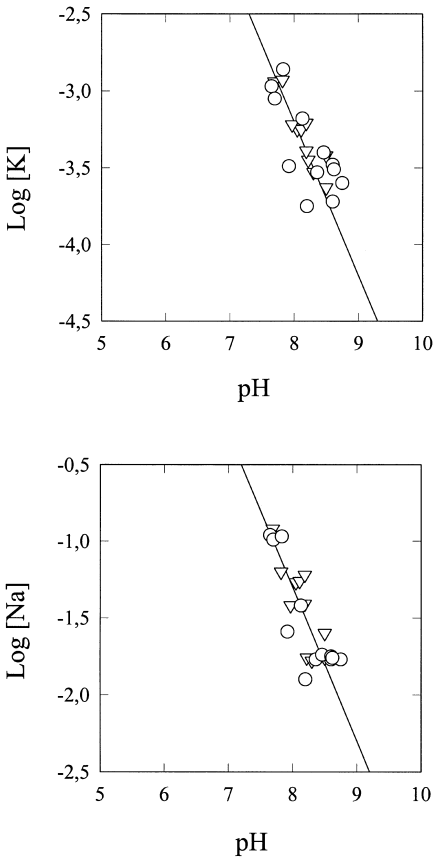

Fig. 13. Correlation of potassium and sodium activities with pH for water in a clay environment. Triangles represent the data of Patyn (1985) and circles those of this work.

variation of the temperature in the aquifer (11–25°C). The log (Na)/(H) and log (K)/(H) constants were estimated as 6.6 ± 1.0 and 4.7 ± 1.0 from the observed correlations and are consistent with a global equilibrium between the solution and the following mineral assemblage: chalcedony, kaolinite, microcline and albite. The observation of new-formed feldspars (principally K-feldspars) in the clayey matrix also points to the existence of this mineral control.

4.3.2. Comprehensive model

The system is assumed to be a solution in contact with a mineral assemblage containing the following elements: Al, Si, Na, K, Ca, Mg, H, O, C and Cl. The O_2 concentration is not an independent variable as it is imposed by the redox states of the other elements. To simplify the calculation, the redox equilibria for the trace elements, mainly Fe and S, are not taken into account in this step. In such a model, two kinds of elements can be distinguished:

- *free elements* the concentration of which in solution is not constrained by the precipitation of a mineral phase. That is essentially the case of the halogens for which the potentially limiting minerals are very soluble. Their concentrations are fixed from outside the system. In the model, the Cl concentration is related to the mixing ratio with the marine endmember.
- *controlled elements* the concentration of which in solution is constrained by the saturation with a mineral phase. It is considered that Si is regulated by chalcedony, Al by kaolinite, Ca by calcite, Mg by dolomite, Na by albite and K by microcline respectively. The dissolution equilibria for these minerals are well characterised, as following:

$$\underset{\text{Chalcedony}}{SiO_2 + 2H_2O \Leftrightarrow H_4SiO_4} \qquad (H_4SiO_4) = K_{chalc} \tag{1}$$

$$\underset{\text{Kaolinite}}{Al_2Si_2O_5(OH)_4 + 7H_2O \Leftrightarrow 2Al(OH)_4^- + 2H_4SiO_4 + 2H^+} \qquad (Al(OH)_4^-)^2 \cdot (H_4SiO_4)^2 \cdot (H^+)^2 = K_{kaol} \tag{2}$$

$$\underset{\text{Calcite}}{CaCO_3 + 2H^+ \Leftrightarrow Ca^{++} + H_2O + CO_2} \qquad (Ca^{++}) \cdot pCO_2/(H^+)^2 = K_{cal} \cdot (K_1.K_2.\alpha)^{-1} \tag{3}$$

where K_1 and K_2 are the acidity constants of carbonic acid and α the coefficient of Henry's law for carbonic acid ($H_2CO_3 = \alpha \cdot pCO_2$).

$$\underset{\text{Dolomite}}{CaMg(CO_3)_2 + 4H^+ \Leftrightarrow Ca^{++} + Mg^{++} + 2H_2O + 2CO_2} \qquad (Ca^{++}) \cdot (Mg^{++}) \cdot pCO_2^2/(H^+)^4 = K_{dol} \cdot (K_1 \cdot K_2 \cdot \alpha)^{-2} \tag{4}$$

$$\underset{\text{Chalcedony}}{\underset{\text{Albite}}{NaAlSi_3O_8 + H^+ 1/2H_2O} \Leftrightarrow \underset{\text{Kaolinite}}{1/2Al_2Si_2O_5(OH)_4 + Na^+ + 2SiO_2}} \qquad (Na^+)/(H^+) = K_{alb} \cdot K_{kaol}^{-1/2} \cdot K_{chalc}^{-2} \tag{5}$$

$$\underset{\text{Chalcedony}}{\underset{\text{Microcline}}{KAlSi_3O_8 + H^+ + 1/2H_2O} \Leftrightarrow \underset{\text{Kaolinite}}{1/2Al_2Si_2O_5(OH)_4 + Na^+ + 2SiO_2}} \qquad (K^+)/(H^+) = K_{mic} \cdot K_{kaol}^{-1/2}.K_{chalc}^{-2} \tag{6}$$

K_{chalc}, K_{cal}, K_{dol}, K_{kaol}, K_{alb} and K_{mic} are the dissolution constants of chalcedony, calcite, dolomite, kaolinite, albite and microcline respectively and are listed in Table 4.

Carbon deserves a special mention because the mechanism of the CO_2 regulation in confined aquifers remains complex. In a series of sedimentary aquifers, the observed CO_2-temperature relationship between 10 and 200°C has been successfully explained by the equilibrium of the fluids with a mineral assemblage constituted by calcite, dolomite and a Mg bearing aluminosilicate (Gouze, 1993; Hutcheon et al., 1993). The last author showed also that additional production of CO_2 by the decomposition of organic matter, which occurs in a rather narrow temperature range (80–120°C according to Smith and Ehrenberg, 1989), does not

Table 4
Comparison of different data banks regarding the logarithms of the hydrolysis constants of aluminate and the principal mineral phases considered in the model. Equilibria are considered with the following species: H^+, Na^+, K^+, Ca^{2+}, Mg^{2+}, CO_3^{2-}, $Al(OH)_4^-$ and H_4SiO_4

	This study	MINTEQ[a,b]	SUPCRT[a,c]	Bowers et al. (1984)	Michard (1983)
Albite (low temp.)	−20.6	−20.41	−21.09	−19.10	−19.98
Chalcedony	−3.71	−3.52	−3.73	−3.73	−3.71
Calcite	+8.16	+8.20	+8.04		+8.16
Dolomite	−17.02	−17.00	−18.30	−18.14	−17.02
Disordered dolomite	−16.60			−16.60	
Microcline	−22.3	−22.38	−24.3	−22.6	−22.12
Kaolinite	−39.16	−40.27	−40.90	−36.97	−39.16
$Al(OH)_4^-$	−23.00	−23.00	−23.00	−23.00	−22.20

[a] These data are from a recent compilation of thermodynamic data for the principal minerals made by Engi (1994).
[b] Ensemble of the USGS data, revised by Nordstrom et al. (1984), and of the MINTEQ code data base (Felmy et al., 1984).
[c] Data taken essentially from Helgeson et al. (1978) and numerous up-dates.

change the CO_2 of the system as it is buffered by the set of minerals. The main problem is to identify and characterise the proper Mg aluminosilicate, as these phases often have an uncertain stoichiometry and the range of variability of their formation constant can be of several orders of magnitude. For example published values of the formation constant of chlorite vary from $10^{-22.57}$ (Bowers et al., 1984) to $10^{-16.16}$ (Michard, 1983). The corresponding CO_2, calculated for the above mentioned buffer, lies between $10^{-3.11}$ and $10^{-1.87}$. This last value is consistent with the data the authors obtained for the Rupelian aquifer. However, as all the waters in this study are in a very narrow range of temperature and as no detailed mineralogical analysis of the silts is available, it is not possible to identify the peculiar Mg–Al–Si phase for this case and to constrain the set of data in this way. Therefore, as the variation of the inorganic C content in the whole aquifer is small, this parameter was fixed in the model.

The principle of the calculation is simple. The concentration of each controlled cation can be expressed as a function of (H^+) and CO_2 using Eqs. (1)–(6). As the total inorganic C concentration is fixed, CO_2 is also a function of (H^+) alone. [Cl] is an independent variable and so the pH results from requiring the solution to be electrically neutral and the overall composition of the solution can then be calculated. The phase rule is respected: a mineral phase is associated with each regulated element.

The PHREEQE computation code (Parkhurst et al., 1980) was used with the database shown in Table 4. In the study, the dissolution constants of albite and microcline were calculated using the slopes of the correlation lines in Fig. 13 and Eqs. (5) and (6). The dissolution constants of the involved minerals in this model are compared with those of different data bases. MINTEQ corresponds to a database well suited to low-temperature equilibria in a natural environment. However, it is the result of a compilation of constants with very different origins that could not always be verified. The SUPCRT base is from a consistent ensemble of high-temperature calorimetric measurements whose results are extrapolated to low temperatures. This can perhaps explain the appreciable differences with respect to the other bases.

4.3.3. Results and discussion

Calculations have been made for all waters. Table 5 shows the results for both endmembers. Curves in Fig. 6 evidence a reasonable agreement between calculated curves and experimental results: the choice made for the mineral assemblage, whose components were observed in the Boom clay (Griffault et al., 1996) but only suspected in the aquifer sands, makes it possible to portray the evolution of the whole set of groundwaters.

Indeed, the choice of the involved mineral assemblage can be critical. In the present case the clay minerals were not taken into account although these phases represent more than 50% in the Boom Clay. The main reason is that the description of dissolution and precipitation equilibria for clay minerals is far from being unambiguous: are the clay minerals, in particular the mixed-layer clays, to be treated as defined phases or solid solutions? The first approach consists in considering average compositions of clay minerals and defining the thermodynamic constants from assemblies of oxide and hydroxides (Tardy and Garrels, 1974). This often leads to more or less accurate and arbitrary limits between the mineral domains. The variability of clay minerals is taken into account in the n-pole solid solution model (Tardy and Fritz, 1981). Aagard and Helgeson (1983) and Giggenbach (1985) simplified this model by limiting the number of poles and described solutions in contact with the clay minerals employing the activity diagrams normally used

in geochemistry. However, none of these models is entirely satisfactory and the great uncertainties involved led the authors to prefer one based on better defined secondary phases.

On the other hand clays are known for their ion-exchange properties. The reserve of exchangeable cations can be considerable, in particular for smectites and illites. For example, 1 kg of humid Boom clay contains 192 meq of exchangeable cations, while only 2.7 meq of the same species are dissolved in the corresponding interstitial water. It might therefore be assumed that ion-exchange reactions could be involved in regulating the clay water composition.

To intend such modelling, it is important to have a precise characterisation of the clay surface, its ion-exchange capacity and its thermodynamic properties. A simple representation (uniform surface, one single type of exchange site per mineralogically 'pure' clay) can explain binary exchanges in limited concentration domains (Sposito et al., 1983; Pitsch et al., 1992) but does not allow dealing with more complex situations, like that of equilibrium with a natural water. The limitations encountered by Thellier and Sposito (1988) in modelling the behaviour of illite towards solutions containing several cations is one of the best examples. Recent work (Gorgeon, 1994) has shown that the 'pure' phases have several sites each characterised by a capacity and a set of exchange constants, and that significant variations of these characteristics are observed from one mineral to another.

Knowledge of all these parameters makes it possible to compute the cationic composition of water in equilibrium with a mineral or a set of minerals having a total of m exchange sites, from the total concentrations of the n exchangeable cations in the clay phase and one of the aqueous phase concentrations or the pH: there are $n\cdot(m+1)-1$ unknowns and an equal number of equations, namely $m+n-1$ mass balances and $m\cdot(n-1)$ mass action laws.

Such a calculation was tested on Boom clay and its interstitial water. Additivity of the exchange capacities of the single minerals including interstratified clays was assumed and the kaolinite fraction was neglected in the computations due to its very low capacity (2.4% of the total). Analysis of the sorption isotherms on the corresponding pure phases (Pitsch et al., 1992; Gorgeon, 1994; Pillette and Ly, 1994) showed that the metal cations are fixed on one illite and one smectite site and the Ca and Mg concentrations in the interstitial water were computed from that of Na: $[Ca]=0.16$ mM and $[Mg]=0.15$ mM. They are somewhat higher than the measured values, 0.048 and 0.07 mM respectively: the simplifying assumptions of the model (simple additivity, representativity of the characterised pure phases), the ignorance of the exact behaviour of K and of the role played by organic matter in complexing the alkaline earths, mean that there are rather large uncertainties in the computed results, which might only be reduced by completing the available set of thermodynamic data.

Indeed it is not surprising that ion exchange equilibrium between the surface of the Boom clay and the interstitial water seems to be achieved, as these reactions are very fast compared to mass transfer kinetics. Nevertheless it must be emphasised that modelling of groundwaters with only ion-exchange reactions appears to be unrealistic. Beyond the mentioned difficulties it is necessary to observe that the type of calculation presented here is not a proper modelling of the water composition. Conversely to the dissolution–precipitation model, which is not dependant on the quantities in the solid (whose activity is by convention equal to one), computing the concentrations in the solution

Table 5
Comparison of the calculated compositions with the measured ones for the interstitial fluid and an aquifer groundwater. All the concentrations are in mmol/l

	Bicarbonated water modelled	Inerstitial water composition	Chloride rich water modelled	Meer 20D water composition
	Fixed parameters	Measured parameters	Fixed parameters	Measured parameters (two runs)
C	11.6		12.4	
Cl	0.5	0.5	94	94–94
	Computed parameters	Measured parameters	Computed parameters	Measured parameters
pH	8.64	8.2–8.6	7.77	7.65–7.70
Alk.	11.9	12	13.2	13.2–13.2
Ca	0.032	0.05	0.34	0.60–0.83
Mg	0.068	0.1	0.75	1.30–1.88
Na	12.3	12.6	104	102–110
K	0.12	0.2	1.06	0.88–1.06
Si	0.2	0.15	0.19	0.22–0.24

from ion-exchange reactions requires one to know the quantity of each regulated cation which is associated to the solid phase. Even then, only ratios of the cations are constrained and to calculate the composition of the solution it is necessary to know the concentration of one dissolved species. A pure ion exchange model is far from being constrained.

4.4. Characterisation of the oxidation–reduction state of the interstitial water

4.4.1. Indirect potential determination

The combined pE-pH diagram for Fe and S (Fig. 14) was plotted for total S and Fe concentrations of 10^{-6} M and 10^{-2} M of total inorganic C, using thermodynamic constants at 25°C from Langmuir (1969); Plummer et al. (1976); Sillen and Martell (1964); Biernat and Robins (1972). It shows the predominance fields of siderite and pyrite. Both solids have been observed in the mineralogical study of the Boom clay, and trace element analysis showed that the interstitial water is saturated with siderite. The clay water potential is, therefore, lower than −220 mV (pE = −3.73).

Analysis for the different S species in the interstitial water was performed, but sulphide as well as thiosulphate concentrations are below the detection limit. If a sulphide concentration of exactly the detection limit (1 μM) is admitted, the H potential value is at most −240 mV (pE = −4.1), the upper limit of the pyrite domain.

Within the CERBERUS project (Beaufays et al., 1994b), measurements of the pH and redox potential on a heated and irradiated fluid were performed. The corresponding point on the diagram falls in the domain where pyrite and siderite coexist.

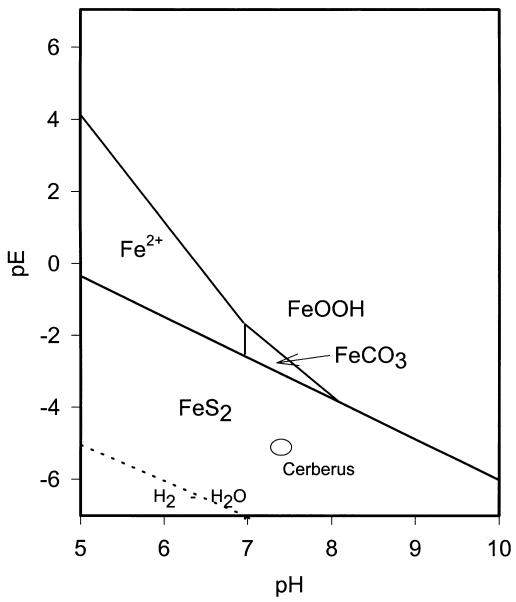

Fig. 14. Combined pE-pH diagram for iron and sulphur at total concentration of 1μM. The circle indicates measurements on in situ heated and γ-irradiated interstitial water obtained by the SCK·CEN team in the european CERBERUS programme.

4.4.2. Modelling of oxidising perturbations

The interstitial water in piezometer No. 1 is characterised by a very low SO_4^{2-} concentration (0.03 mM), whereas in piezometer No. 2 it reaches 10 mM in the first few metres from the gallery. At 15 m, the concentration falls again to 0.1 mM, comparable to that measured in piezometer No. 1. This perturbation observed with piezometer No. 2 is certainly due to oxidation of the medium during the installation of the tubing. Piezometer No. 1 was sterilised at room temperature with formaldehyde, while the second one was sterilised by heating before insertion in the massif, which resulted in oxidation of the pyrite in contact with the hot tubing, air and water. In the pyrite-rich clay massif any oxidation results in a SO_4^{2-} enrichment of the water by the following reaction:

$$FeS_2 + 7/2\,O_2 \rightarrow Fe^{3+} + 2\,SO_4^{2-} + 2H^+$$

However, the oxidation proceeds gradually and the system is rapidly buffered: SO_4 production does not exceed 15 mM and the measured alkalinity remains around 15 mM, while a strong oxidation without reequilibration of the system would produce an acid pH and a drop in the alkalinity equal to twice the SO_4 increase. This reequilibration results from the dissolution of calcite and dolomite in the clay combined with ion exchange reactions between the alkaline earths and the Na fixed on the clay surface. The resulting water contains Na_2SO_4 and $NaHCO_3$.

In addition, filtrations were made at the piezometer outlet and the filters were examined by scanning electron microscopy. The particles retained at the first filtration step at 450 nm were essentially small neo-formed barite crystals, while on the second stage filter (100 nm porosity), numerous S particles associated with organic matter were observed. At this moment, we do not known if this S is the necessary molecular intermediate in pyrite formation, according to the reaction (Berner, 1984):

$$FeS + S \rightarrow FeS_2$$

or if it is chemically bound to the organic matter. In any case, it seems to be readily available for oxidation, as shown by the formation of barite.

4.5. Trace elements behaviour

4.5.1. General concepts

To study the behavior of the very dilute transition metals in groundwaters it is important to evaluate the exact meaning of the analytical data. It is important to distinguish the particulate fraction from the 'soluble' component and a description of the speciation of the element in solution is absolutely necessary for control modelling. The former problem was solved by the improvement of filtration techniques (see Section 2.2). On the other hand, the complexing constants of the main inorganic ligands present in the water samples (OH^-, HCO_3^- and Cl^-) with the majority of the trace metals are well known. The same is not true for the organic molecules, which are often difficult to identify and seldom well characterised.

Thus, the authors have determined the total metal concentration in each of the filtration fractions and obtained the free cation concentration by speciation calculations whenever it was possible. For some elements, a gross approach to the free or weakly bound cations in groundwater was obtained by performing nondestructive analysis (cathodic stripping voltammetry, molecular spectrometry) on samples before and after organic matter destruction by UV irradiation or persulphate digestion.

4.5.2. Results

4.5.2.1. Iron and manganese. Dissolved Fe in reducing groundwaters is present as Fe (II). In fact, Fe (III) is very unstable in solutions close to neutrality and rapidly precipitates as oxides or hydroxides. In the aquifer water as in the interstitial water, the Fe and Mn concentrations are relatively high (around 1 μM). From speciation calculations, dissolved species are Fe^{2+}, $FeCO_3$, $FeHCO_3^+$ and Mn^{2+}. The interstitial water and most aquifer waters are close to saturation with siderite and rhodocrosite. However the water with the highest Cl content (Oelegem and Meer) and the water from the Wuustwezel and Kontich boreholes seemed to be undersaturated with respect to these minerals. In fact, a $Fe(OH)_3$ deposit was observed during the filtration in spite of all the precautions taken in the collecting and filtration procedures; the loss of Fe by oxidation and precipitation could explain the apparent undersaturation with respect to carbonate minerals.

4.5.2.2. Uranium. For a given water, the measured U concentration is the same in all filtration fractions and does not vary after UV irradiation of the samples; this proves that the U is entirely in the 'soluble' fraction and is not associated with organic matter. The main species in the fluids are uranyl–carbonate complexes.

4.5.2.3. Aluminium. The use of sequential filtrations made it possible to determine the soluble Al fraction, for which the data obtained in the ultrafiltered samples at 10 nm are representative. The authors have shown that the waters studied here are close to saturation with kaolinite, while our first measurements on directly ultrafiltered samples, without prefiltration, overestimated the Al concentrations because of particulate contamination, which resulted in an apparent oversaturation with respect to kaolinite.

4.5.2.4. Nickel and cobalt. For samples as a whole, taking analytical errors into account, the concentrations measured in each filtration fraction are equal, indicating that these elements are dissolved. However, the measured Ni and Co concentrations are often close to the detection limit, estimated at twice the concentration of the filtration blank. Thus, only the results from two boreholes, Meer and Mol 15B, are really significant.

A slight increase of the measured concentration with decreasing filter porosity is noted in the Meer sample. This 'concentration' effect is often induced by a modification of the distribution of species in solution, because the enrichment in the supernatant fluid of a fraction strongly retained by the filter surface can displace the solution equilibria to the profit of the free metal passing into the ultrafiltrate (Buffle et al., 1992).

For Mol sample 15B, the Co signal increases after UV irradiation (from 0.15 to 0.65 μg/l) indicates a strong interaction of organic matter with this metal. The same phenomenon occurs with Ni.

4.5.2.5. Lithium, rubidium and strontium. The Sr concentrations vary from 10^{-6} M in the interstitial water to some 10^{-5} M in the aquifer water, following the mixture line with the marine component. The same behaviour is observed for Li and Rb, with concentrations between 10^{-8} and 10^{-7} M. Except for Lommel and Wuustwezel, the water is saturated with $SrCO_3$.

4.5.2.6. Barium. Except for the interstitial water and the Lommel borehole, all the water samples are close to saturation with barite. Paradoxically, examination of the 0.45 μm porosity filters obtained from interstitial water indicates the presence of relatively important amounts of automorphic barite crystals. The latter could be attributed to partial oxidation, during the filtration, of S associated with organic matter, producing a loss of Ba in the filtration phase. In the Lommel borehole, the fluids are in near saturation with $BaCO_3$.

4.5.2.7. Boron. The concentrations of B in solution vary from 10^{-4} M in the surface water to 10^{-3} M in the water with the highest Cl concentrations and in the interstitial water. As for Br, an enrichment of the inter-

stitial water with respect to the marine contribution is observed.

As a rule, these trace elements indicate very clearly the marine origin of the fluids. All the mineral dissolution or reprecipitation processes are in this case masked by this marine contribution, while the behaviour of the major elements provides evidence of reequilibration with the host rock.

5. Conclusion

To support the modelling work, both precise and accurate analytical data were needed. A determining factor to meet this requirement was the strict control of the whole process from the field sampling to the final analysis in the laboratory. As the examined fluids are particularly sensitive to perturbations, a sequential anaerobic filtration procedure was set up, and sample conservation and analytical methods had to be carefully validated. An in situ measurement technique for pH was developed in order to characterise the acidity level of the mudrock fluid, which is no longer buffered outside of the host rock. When it was not possible to perform direct measurements, indirect methods could be demonstrated to be powerful, for example for the characterization of the oxidation–reduction state of the water and the speciation of some metallic ions.

The data interpretation shows that all the examined fluids belong to a coherent ensemble; the origin, acquisition and evolution of their chemical composition has been described in terms of a two endmember mixture of clayey and marine water followed by reequilibration with the host rock. In continuity with previous work on granite water (Grimaud et al., 1990) a predictive model based on dissolution–precipitation equilibria allowed the composition of equilibrated waters to be explained. The concentration of most major elements is controlled by a set of secondary mineral phases, the pH of the fluid depending on the concentration of the 'free' halides. Trace element concentrations seem to result essentially from the mixture of both types of waters but some geochemical controls on trace chemistry by carbonates and organic matter were identified. The concentrations of other elements like Rb and B are not regulated.

It was also shown that the modifications of the water chemistry resulting from an oxidising perturbation can be explained taking into account fast processes like carbonate dissolution and ion-exchange reactions on the clay surface. Due to the lack of a precise thermodynamic description of clayey phases, quantitative predictions are not yet possible but reaction mechanisms are quite well understood.

This work shows that the prediction of the composition of a groundwater hosted by a sedimentary rock is possible in equilibrated and perturbed conditions. It gives preliminary information on the behaviour of relevant elements for the performance assessment of a deep underground storage facility for radioactive waste. New thermodynamic data are necessary to overcome the limitations pointed out. Further research must include the regulation of inorganic C concentration and redox potential, complexing properties of the organic matter and ion-exchange properties of the surface-sorbing mineral phases, in order to predict the consequences of a possible release from an underground storage facility. An extension of the data base built up within the present work, including other aquifers and especially concerning trace elements, is foreseen with the purpose of completing the model assessment and contributing to the interpretation of the regional hydrodynamics with the aid of chemical and isotopic indicators. Use of the model in interpreting data from other sedimentary aquifers and aquitards will be used for complete validation.

Acknowledgements

This work was financed by the European Communities' Commission and the french Agence nationale de gestion des déchets radioactifs, within the ARCHIMEDE - Argile project (contract F12W-CT92-0117, Griffault et al., 1996). The authors are grateful to all other participants of this programme, especially to Pierre De Cannière, as well as to Marie Claude Magonthier for fruitful scientific discussion. They wish to thank Pascal L'Hénoret, Claudine Mandon, Claude Boursat, Nathalie Trésonne and Alexandre Beltriti for technical help. The skillful contribution of Rudy Beaufays and André Fonteyne from SCK·CEN during the sampling and measurement campaigns are also acknowledged.

References

Aagard, P., Helgeson, H.C., 1983. Activity composition relations among silicates and aqueous solutions, II: chemical and thermodynamical consequences of ideal mixing of atoms on homological sites in montmorillonites, illites, and mixed-layer clays. Clays Clay Miner. 31, 207–217.

Araguas, L., Rozanski, K., Gonfiantini, R., Louvat, D., 1995. Isotope effects accompanying vacuum distillation extraction of soil water for stable isotope analyses. J. Hydrol. 168, 159–171.

Beaucaire, C., Toulhoat, P., Pitsch, H., 1995. Chemical characterisation and modelling of the interstitial fluid in the Boom clay Formation. In: Proc. 8th Internat. Symp. Water–Rock Interaction (WRI-8), Vladivostok, Russia, pp. 779–782.

Beaufays, R., Bloomaert, W., Bronders, P., De Canniere, P., Del Marmol, P., Henrion, P., Monsecour, M., Patyn, J., Put, M., 1994. Characterisation of the Boom clay and its multilayered hydrogeological environment. Final report, Project EUR 14961 EN.

Beaufays, R., De Cannière, P., Fonteyne, A., Labat, S.,

Meynendonckx, L., Noynaert, L., Volckaert, G., Bruggemen, A., Lambrechts, M., Vandervoort, F., 1994. CERBERUS: a demonstration test to study the near field effects of an HLW canister in an argillaceous formation. Report EUR 15718 EN.

Berner, J., 1984. Sedimentary pyrite formation: an update. Geochim. Cosmochim. Acta 48, 605–615.

Biernat, R.J., Robins, R.G., 1972. High temperature potential-pH diagrams for the iron–water and iron–water–sulphur systems. Electrochim. Acta 17, 1261.

Boisde, G., Perez, J.J., 1988. European patent No. 284.513.

Bowers, T.S., Jackson, K.J., Helgeson, H.C., 1984. Equilibrium Activity Diagrams. Springer-Verlag.

Buffle, J., Perret, D., Newman, M., 1992. The use of filtration and ultrafiltration for size fractionation of aquatic particles, colloids and macromolecules. In: Buffle, J., Van Leeuven, H.P. (Eds.), Environmental Particles, vol. 1. Lewis Publishers.

Covington, A.K., Bates, R.G., Durst, R.A., 1985. Definition of pH scales, standard reference values, measurement of pH and related terminology. Pure Appl. Chem. 57, 531–542.

Engi, M., 1994. Thermodynamic data for minerals: a critical assessment. In: Price, G.D., Ross, N.L. (Eds.), The Stability of Minerals. Chapman and Hall.

Felmy, A.R., Girvin, D.C, Jenne, E.A., 1984. MINTEQ: a computer program for calculating aqueous geochemical equilibria. EPA-600/3-84-032, US Environmental Protection Agency, Atlanta, Georgia. (NTIS PB84-157148, National Technical Service, Springfield, Virginia).

Fontes, J.Ch., Matray, J.M., 1993. Geochemistry and origin of formation of brines from the Paris basin, France. Chem. Geol. 109, 149–200.

Gorgeon, L., 1994. Contribution à la modélisation physico-chimique de la rétention de radioéléments à vie longue par des matériaux argileux, PhD Thesis, Univ. Paris 6.

Giggenbach, W.F., 1985. Construction of thermodynamic stability diagrams involving dioctahedral potasium clay minerals. Chem. Geol. 49, 231–242.

Gouze, P., 1993. Modélisation des transferts de masse liés aux circulations dans les aquifères sédimentaires. Application à l'aquifère du Dogger du Bassin de Paris et aux écoulements thermo-convectifs dans les réservoirs gréseux, PhD thesis, Univ. Paris 6.

Griffault, L., Merceron, T., Mossmann, J.R., Neerdael, B., De Canniere, P., Beaucaire, P., Daumas, S., Bianchi, A., Christen, R., 1996. Projet 'ARCHIMEDE - argile': Acquisition et régulation de la chimie des eaux en milieu argileux pour le projet de stockage de déchets radioactifs en formation géologique. Rapport EUR 17454 FR.

Grimaud, D., Beaucaire, C., Michard, G., 1990. Modelling the evolution of ground waters in a granite system at low temperature: the Stripa ground waters, Sweden. App. Geochem. 5, 515–525.

Helgeson, H.C., Delany, J.M., Nesbitt, H.W., Bird, D.K., 1978. Summary and critique of the thermodynamic properties of rock forming minerals. Amer. J. of Sci. 278A, 1–229.

Hutcheon, I., Shevalier, M., Abercrombie, H.J., 1993. pH buffering by metastable mineral fluid equilibria and evolution of carbon dioxide fugacity during burial diagenesis. Geochim. Cosmochim. Acta 57, 1017–1027.

IAEA, 1992. Statistical treatment of data and environmental isotopes in precipitations. Technical Report Series 331.

Langmuir, D., 1969. The Gibbs free energies of substances in the system $Fe–O_2–H_2O–CO_2$ at 25°C. US Geol. Surv. Prof. Paper 650B, B180–B184.

Liyuan Liang, McNabb, J.A., Paulk, J.M., Baohua Gu, McCarthy, J.F., 1993. Kinetics of Fe (II) oxygenation at low partial pressure of oxygen in the presence of natural organic matter. Environ. Sci. Technol. 27, 1864–1870.

Michard, G., 1983. Recueil des données thermodynamiques concernant les équilibres eaux-minéraux dans les réservoirs hydrothermaux. Rapport EUR 8590 FR.

Motellier, S., Noire, M.H., Pitsch, H., Dureault, B. pH Determination of Clay Interstitial Water Using a Fiber-Optic Sensor. Sensors Actuators, Part B (in press).

Nordstrom, D.K., Valentine, S.D., Ball, J.W., 1984. Partial compilation and revision of basic data in the WATEQ programs. US Geol. Surv. Water-Resour. Investigation Report 84-4186, 10–14.

Parkhurst, D.L., Thorstenson, D.C., Plummer, L.N., 1980. PHREEQE: a computer program for geochemical calculations, USGS Water resources investigations 80-96, 210 pp.

Patyn, J., 1985. Contribution à la recherche hydrogéologique liée à l'évacuation de déchets radioactifs dans une formation argileuse, Ph.D. thesis, School of Mines, Paris.

Pillette, F., Ly, J., 1994. Pers. comm.

Pitsch, H., Ly, J., Stammose, D., Kabare, I., Lefevre, I., 1992. Sorption of major cations on pure and composite clayey materials. Appl. Clay Sci. 7, 239–243.

Pitsch, H., Motellier, S., L'henoret, P., Boursat, C., 1995a. Characterisation of deep underground fluids, part I: pH determination in a clayey formation. In: Proc. 8th Internat. Symp. Water–Rock Interaction (WRI-8), Vladivostok, Russia, pp. 467–470.

Pitsch, H., L'henoret, P., Boursat, C., De Canniere, P., 1995b. Characterisation of deep underground fluids, part II: redox potential measurements. In: Proc. 8th Internat. Symp. Water–Rock Interaction, (WRI-8), Vladivostok, Russia, pp. 471–475.

Plummer, L.N., Truesdell, A.D., Jones, B.F., 1976. WATEQF: a fortran IV version of WATEQ: a computer program for calculating chemical equilibrium of natural waters, US Geol. Survey Water Res. J. 76(13).

Robinson, R.A., 1980. Buffer solutions: operational definitions of pH. In Handbook of Chemistry and Physics, 61st ed., CRC Press, D148.

Sillen, L.G., Martell, A.E., 1964. Stability constants of metal-ion complexes. In: Special Publication, 17. Chem Soc, London.

Smith, T.M., Ehrenberg, S.N., 1989. Correlation of carbon dioxide abundance with temperature in clastic hydrocarbon reservoirs: relationship to inorganic chemical equilibrium. Mar. Pet. Geol. 6, 129–135.

Sposito, G., Holtzclaw, K.M., Charlet, L., Jouany, C., Page, A.L., 1983. Sodium–calcium, sodium–magnesium and calcium–magnesium exchange on Wyoming bentonite at 298°K. Soil Sci. Soc. Am. J. 47, 51–56.

Tardy, Y., Garrels, R.M., 1974. A method of estimating the Gibbs energy of formation of layer silicates. Geochim. Cosmochim. Acta 38, 1101–1116.

Tardy, Y., Fritz, B., 1981. An ideal solid solution model for calculating solubility of clay minerals. Clay Miner. 16, 361–373.

Thellier, C., Sposito, G., 1988. Quaternary exchange on Silver Hill illite. Soil Sci. Soc. Am. J. 52, 979–985.

Vandenberghe, N., Van Echelpoel, E., 1987. Field guide to the Rupelian stratotype. Bull. Soc. Belge Géol. 96, 325–337.

Wouters, L., Vandenberghe, N., 1994. Géologie de la campine, ONDRAF/NIRAS ed., Nirond 94–12.